2015 American Control Conference
Palmer House Hilton
July 1-3, 2015. Chicago, IL, USA

A Longitudinal Spatial Coherence Model for Wind Evolution based on Large-Eddy Simulation

Eric Simley[1] and Lucy Y. Pao[2]

***Abstract*— Standard feedback controllers on wind turbines can be augmented with feedforward control, relying on preview measurements of the wind provided by remote sensing instruments, to help regulate rotor speed and reduce structural loads. The effectiveness of feedforward control depends on how accurately the approaching wind can be measured. One significant cause of measurement error is the evolution of the wind as it travels toward the turbine from the measurement location. Wind evolution is commonly quantified using longitudinal spatial coherence to describe the decorrelation of turbulence as the wind advects downstream. In this paper, a collection of wind fields produced by large-eddy simulation is used to calculate longitudinal coherence for a variety of atmospheric conditions. Using the calculated coherence curves, we determine a simple longitudinal coherence formula for approximating wind evolution, which depends on mean wind speed, turbulent kinetic energy, and turbulence length scale. This formula is then used to find the optimal scan configurations that minimize measurement error for a preview-based control scenario employing Light Detection and Ranging. Results show how the optimal preview distance and achievable measurement error depend on the aforementioned wind parameters.**

I. Introduction

By utilizing measurements of the approaching wind speeds provided by Light Detection and Ranging (lidar), preview-based wind turbine control systems are capable of improving rotor speed regulation and reducing structural loads [1]–[4]. The wind disturbance that will interact with the turbine rotor cannot be measured perfectly, however. For example, a circularly-scanning lidar located in the hub of a wind turbine [5] can only measure the line-of-sight velocity, as opposed to the true longitudinal wind component, which has the greatest impact on the rotor aerodynamics. Furthermore, rather than measuring the wind at a single point, lidars detect wind speeds that are spatially averaged along the beam direction [6]. Another important source of error is wind evolution, or the change in the wind speeds between the time they are measured and when they reach the turbine.

An example of a preview-based control scenario using lidar measurements is shown in Fig. 1. A feedback control loop using blade pitch actuation to regulate rotor speed (and generated power) in above-rated conditions is augmented with a blade pitch feedforward controller designed to cancel the impact of the rotor effective wind disturbance u_{eff} on rotor speed using lidar measurements of the approaching wind. However, wind evolution causes the wind speeds measured by the lidar to differ from those that reach the turbine. A prefilter H_{pre} can be employed to remove components of the lidar measurements that are uncorrelated with the wind that reaches the rotor, improving the accuracy of the wind speed estimates $\hat{u}_{eff}$ and preventing unnecessary or harmful feedforward control actions [7]. Knowledge of the properties of wind evolution can help with the design of such prefilters as well as with the design of lidar measurement strategies that maximize measurement correlation.

In early research on preview-based wind turbine control, Taylor's frozen turbulence hypothesis was assumed [1], [4]. That is, turbulence measured upstream of the turbine was assumed to arrive at the turbine unchanged after traveling downstream at the mean wind speed. More recent preview-based control evaluations have begun to include wind evolution, often modeled using functions describing the coherence between wind speeds separated longitudinally in the flow [3], [4], [8]–[10]. A simple exponential decay coherence formula proposed by Davenport [11] and extended to the longitudinal direction by Pielke and Panofsky [12], which depends on the product between wavenumber, longitudinal separation, and a decay parameter, has been used to introduce wind evolution to calculations of the coherence between lidar measurements and the wind that reaches the rotor [9]. An analytic expression for longitudinal coherence in neutral atmospheric conditions, derived by Kristensen [13], has been used to create four-dimensional stochastic wind fields for assessing the impact of wind evolution on lidar-based control [3], [4]. While the Kristensen model depends on atmospheric

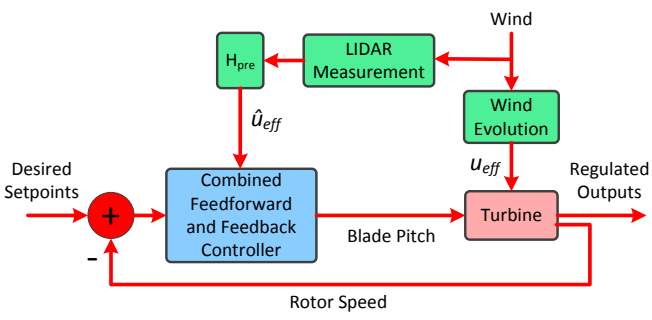

Fig. 1. Block diagram of a combined feedback/feedforward wind turbine control system utilizing a prefilter H_{pre} to provide an estimate of the rotor effective wind speed u_{eff} from lidar measurements.

This work was supported by the US National Renewable Energy Laboratory (NREL). The authors wish to thank Paul Fleming at NREL for providing the large-eddy simulation data used to calculate the longitudinal coherence curves presented in this paper.

[1]Eric Simley is a doctoral candidate in the Dept. of Electrical, Computer, and Energy Engineering, University of Colorado, Boulder, CO 80309, e-mail: eric.simley@colorado.edu

[2]Lucy Y. Pao is the Richard & Joy Dorf Professor in the Dept. of Electrical, Computer, and Energy Engineering, University of Colorado, Boulder, CO 80309, e-mail: pao@colorado.edu

parameters, it has not been validated by field measurements or computational fluid dynamics (CFD) simulations.

In this paper, longitudinal coherence curves are calculated for a collection of wind fields representing a variety of mean wind speeds, turbulence intensities, and atmospheric stability categories generated using large-eddy simulation (LES), a type of CFD. The LES wind fields were provided by the National Renewable Energy Laboratory (NREL), and were generated using NREL's SOWFA tool [14]. We then fit a simple coherence model, based on a formula for transverse and vertical coherence developed by Thresher *et al.* [15], to the calculated coherence curves and determine how the model parameters depend on atmospheric conditions. It is found that the coherence model can be well-fit to the calculated LES coherence curves using mean wind speed, turbulent kinetic energy, and integral length scale as model parameters. The longitudinal coherence model is then combined with a stochastic frequency-domain wind field model [16] to calculate the optimal preview distance, scan radius, and measurement error for a hub-mounted circularly-scanning lidar scenario as a function of mean wind speed and turbulence intensity.

The remainder of the paper is organized as follows. A description of the twelve LES wind fields generated using SOWFA is provided in Section II. Coherence curves calculated from the LES data as well as the description of the longitudinal coherence model fit to the curves are presented in Section III. In Section IV, a circularly-scanning lidar measurement scenario involving the NREL 5-MW wind turbine model [17] is described. Using the developed wind evolution model, the minimum-error lidar scan parameters are found for a range of atmospheric parameters. Finally, Section V concludes the paper with a discussion of the results and proposed model improvements.

II. Large-Eddy Simulation Wind Fields

A collection of twelve LES wind fields provided and generated by NREL is used to determine longitudinal spatial coherence curves for a variety of wind conditions. The wind fields were generated using NREL's SOWFA tool [14], which combines a CFD solver based on OpenFOAM [18] with NREL's FAST aeroelastic code to simulate the two-way interaction between the atmospheric boundary layer and a turbine. Note that in this study, only the LES portion of SOWFA is utilized; there are no wind turbines located in the sections of the wind field analyzed. A domain volume of 3 km $\times$ 3 km $\times$ 1 km was used to develop the atmospheric boundary layers. To reduce the computational time, a grid resolution of 12 m was used for most of the domain, but the wind speeds analyzed are located in a 3 m-resolution grid refinement zone. Although time steps of 0.02 s were used during simulation, the data analyzed here are only sampled once per second. The final wind field segments used to calculate coherence curves in this study are horizontal planes at a height of 90 m (hub height for the NREL 5-MW reference turbine model used in the analysis in Section IV) extending 385 m in the longitudinal along-wind (x) direction and 370 m in the transverse (y) direction. While the original LES simulations were generated for thousands of seconds to allow boundary layer development, the segments used for analysis range from 470 to 670 s.

Of the twelve wind conditions simulated, half contain approximately 8 m/s mean wind speeds (wind field IDs 1–6) and half contain approximately 12 m/s mean wind speeds (IDs 7–12). For both mean wind speed categories, neutral, unstable, and stable conditions were simulated for both a low turbulence case representative of offshore conditions [19], implemented using a surface roughness of $2 \cdot 10^{-4}$ m, and a high turbulence case representative of onshore conditions, using a surface roughness of 0.2 m. The unstable cases were generated using a surface heating rate of 1 K/hr while the stable wind fields contain a heating rate of -1 K/hr. Further information about SOWFA and the LES simulation environment can be found in [19] and [20]. Additional details for all wind fields are provided in Table I, including the turbulent kinetic energy, the integral length scale of the longitudinal u component, and the u component turbulence intensity TI_u, defined as the standard deviation of u expressed as a percentage of the mean wind speed. Turbulent kinetic energy (TKE) is equivalent to

$$\mathrm{TKE} = \frac{1}{2}\left(\sigma_u^2 + \sigma_v^2 + \sigma_w^2\right) \tag{1}$$

where σ_u^2, σ_v^2, and σ_w^2 are the variances of the u component, transverse v component, and vertical w component, respectively, of the wind velocity. The integral length scale L_u is defined as

$$L_u = U \int_0^\infty R_{uu}(\tau)\, d\tau \tag{2}$$

where $R_{uu}(t)$ is the autocorrelation function of the u velocity as a function of time [21] and U is the mean wind speed. The length scales in this paper were calculated by integrating $R_{uu}(t)$ up to the first zero crossing. Examples of planes of instantaneous wind speeds for all three stability classes in the $U \approx 12$ m/s, high turbulence category are provided in Fig. 2, where the different length scales can be compared.

TABLE I

Details of the twelve LES wind fields (IDs 1 through 12) including mean wind speed (U), stability (N: neutral, U: unstable, S: stable), turbulent kinetic energy, u component integral length scale, and u component turbulence intensity (TI_u). All statistics are for a height of 90 m.

ID	U (m/s)	Stab.	TKE (m/s)	L_u (m)	TI_u (%)
1	8.0	N	0.20	71	5.5
2	8.0	U	0.44	178	6.9
3	8.0	S	0.03	28	2.1
4	8.2	N	0.72	96	10.3
5	8.2	U	1.73	241	12.8
6	8.0	S	0.13	33	4.7
7	12.0	N	0.38	115	5.3
8	12.2	U	1.05	211	7.3
9	11.9	S	0.20	42	3.9
10	11.7	N	1.65	186	11.8
11	10.6	U	2.08	230	14.1
12	11.9	S	0.93	56	8.5

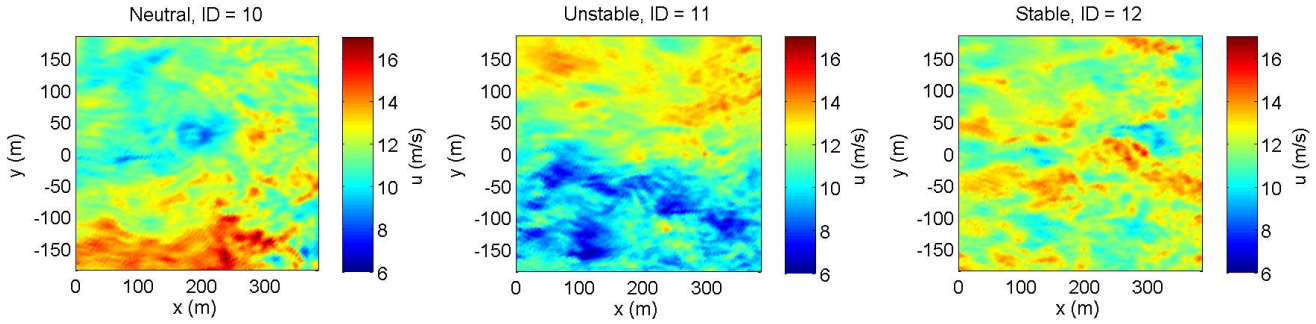

Fig. 2. Examples of instantaneous u velocities in neutral, unstable, and stable LES wind fields (IDs 10, 11, and 12) at a height of 90 m with mean wind speeds of approximately 12 m/s and u component turbulence intensities of 11.8%, 14.1%, and 8.5%, respectively.

III. Longitudinal Coherence Model

This section contains a discussion about how longitudinal coherence curves describing wind evolution are calculated from LES wind fields as well as a description of the longitudinal coherence model based on the LES calculations.

A. Longitudinal Coherence from LES Wind Fields

Coherence describes the correlation between two time-domain signals as a function of frequency, taking on values between 0 (no correlation) and 1 (perfect correlation). Magnitude squared coherence between two signals x and y, the form used in this paper, is defined as

$$\gamma_{xy}^2(f) = \frac{|S_{xy}(f)|^2}{S_{xx}(f)\,S_{yy}(f)} \tag{3}$$

where $S_{xy}(f)$ is the cross-power spectral density between x and y and $S_{xx}(f)$ and $S_{yy}(f)$ are the power spectral densities (PSDs) of signals x and y [21]. Wind evolution is described here using the coherence between the wind speeds at locations separated a distance d_ℓ in the longitudinal mean wind direction. If turbulence were to remain frozen, then the longitudinal coherence would take on a value of 1 at all frequencies and d_ℓ separations. Only wind evolution for the u component is analyzed in this work. All coherence curves discussed here were calculated using Welch's modified periodogram method [21] with a Hamming window and 120 s data segments. The spectra are calculated using 550 pairs of wind speed time-series separated by a longitudinal distance of d_ℓ within the wind field planes. Examples of longitudinal coherence curves calculated for LES wind conditions representing the three stability cases are shown by the black curves in Fig. 3 for pairs of wind speeds at points i and j with d_ℓ = 31.5 m, 63 m, 126 m, and 252 m, equivalent to 0.25, 0.5, 1, and 2 rotor diameters (D = 126 m) for the NREL 5-MW reference turbine. Coherence decreases as the longitudinal separation increases because the wind has more time to evolve. Coherence also decreases with increasing frequency, indicating that the high-frequency, small turbulence scales decay faster than the low-frequency, large scales.

B. Development of a Longitudinal Coherence Model

An attempt was made to fit the two longitudinal coherence formulas used in the lidar-based controls literature, and discussed in the introduction, to the LES-based coherence curves. Values of the unitless decay parameter presented by Pielke and Panofsky [12] for the exponential decay model range from approximately 10 to 50, and produce values of coherence that are much too low compared to the calculated values. Schlipf *et al.* [9] find that a decay parameter of 0.4 matches field measurements quite well, but it is unclear how the parameter depends on turbulence statistics. Contrarily, when using values of TKE and L_u calculated from the LES data, the Kristensen model [13] overestimates the coherence. An additional problem with these two models is that as

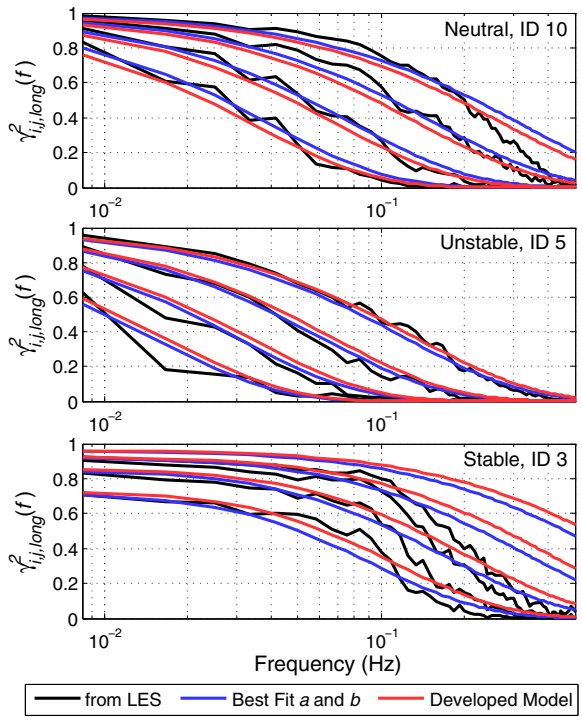

Fig. 3. Longitudinal coherence curves for wind field IDs 10 (neutral, high wind speed, high turbulence), 5 (unstable, low wind speed, high turbulence), and 3 (stable, low wind speed, low turbulence). Coherence curves calculated from the LES wind fields are compared with the coherence formula in (4), using the best fit a and b parameters for each wind field, and the coherence model in (7) using a_1 =8.4, a_2 = 0.05, b_1 = 0.25, and b_2 = 1.24. Ordered from top to bottom in each plot, the coherence curves are for longitudinal separations of d_ℓ = 31.5 m, 63 m, 126 m, and 252 m.

frequency approaches zero, coherence always approaches 1, but as is evident in the stable coherence curves in Fig. 3, this is not always realistic. A suitable coherence model should therefore allow for non-unity coherence at 0 Hz (DC).

The coherence formula developed by Thresher [15] for transverse and vertical separations and included in various forms in the IEC standard [22] and NREL's TurbSim stochastic wind field generator [16] contains a parameter that creates a bias at DC preventing coherence from approaching 1. This coherence formula, with d_ℓ representing the separation distance between wind speeds at points i and j in the transverse and vertical plane in the original definition [15], but indicating a longitudinal separation distance when applied here as a longitudinal coherence function, is defined as

$$\gamma_{i,j}^2\left(f, d_\ell\right) = \exp\left(-a\sqrt{\left(\frac{f d_\ell}{U}\right)^2 + \left(b d_\ell\right)^2}\right) \tag{4}$$

with a and b serving as tuning parameters. When b = 0, (4) is identical to the Pielke and Panofsky model. To determine if (4) is a suitable formula, the expression is fit to the LES-based coherence curves by tuning a and b. For each wind condition, a pair of a and b parameters is chosen by minimizing the following objective function:

$$J\left(a,b\right) = \frac{1}{\int_0^{f_{max}} S_{uu}\left(f\right) df} \sum_{k=1}^{N} \int_0^{f_{max}} S_{uu}\left(f\right) \times \left(\gamma_{i,k}^2\left(f, d_{\ell,k}\right) - \gamma_{i,k,\mathrm{LES}}^2\left(f, d_{\ell,k}\right)\right)^2 df. \tag{5}$$

The objective function in (5) sums the integrated square errors between the LES-based calculated coherence curves and the longitudinal coherence formula $\gamma_{i,k}^2\left(f, d_\ell\right)$ in (4), weighted by the power spectrum $S_{uu}\left(f\right)$ of the u component calculated from the LES wind data, over N different longitudinal separations. An integration limit of f_{max} = 0.5 Hz, equal to half the sampling frequency of the LES data, is used. Weighting the errors by the PSD helps ensure that errors are low at the frequencies where most of the power in the wind is concentrated. The sum of the errors is normalized by the integral of $S_{uu}\left(f\right)$ so that values of $J\left(a,b\right)$ for different wind conditions can be meaningfully compared. The three longitudinal separations of $d_\ell = \{63\ \mathrm{m}, 126\ \mathrm{m}, 252\ \mathrm{m}\}$ (0.5 D, 1 D, and 2 D for the NREL 5-MW reference turbine) were chosen for the objective function because earlier research indicates that the optimal measurement distance for preview-based control applications is likely to fall in this range [6], [10]. Examples of the resulting best fit coherence curves are shown by the blue curves in Fig. 3.

The best fit a and b parameters found using (5) were compared with several atmospheric variables calculated from the LES wind fields to determine their relationship to the wind conditions. It was found that a is a strong linear function of the ratio between σ and U, where σ, which is included in the Kristensen model, is equal to $\sqrt{2 \cdot \mathrm{TKE}}$:

$$\sigma = \sqrt{\sigma_u^2 + \sigma_v^2 + \sigma_w^2}. \tag{6}$$

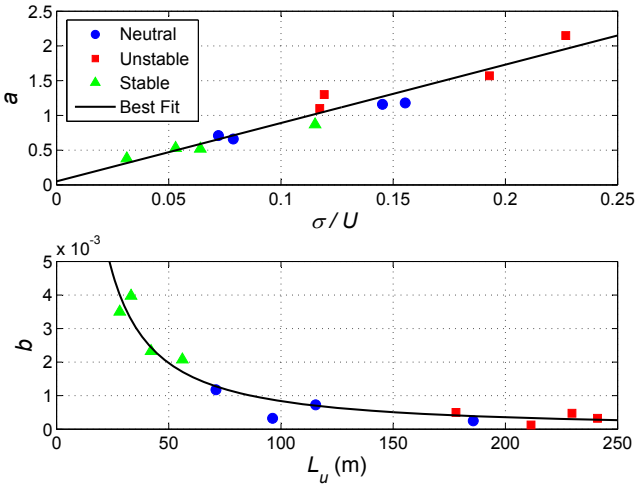

Fig. 4. Best fit a and b coherence parameters from (4) for all twelve wind fields separated by stability class along with the best fit curves describing a as a function of σ/U and b as a function of L_u.

The b parameter, which determines the value that the coherence approaches as frequency approaches 0, appears to be strongly proportional to the inverse of the u component integral length scale. Fig. 4 contains the best fit a and b parameters organized by stability class as functions of σ/U and L_u, respectively. Along with the best fit parameters, Fig. 4 shows the best fit curves relating a and b to σ/U and L_u. The a parameter is described as $a = a_1\sigma/U + a_2$ and b is expressed in a power-law form: $b = b_1 L_u^{-b_2}$. The final form of the developed longitudinal coherence function is given as:

$$\gamma_{i,j,long}^2\left(f, d_\ell\right) = \exp\left(-\left(a_1\frac{\sigma}{U} + a_2\right)\sqrt{\left(\frac{f d_\ell}{U}\right)^2 + \left(b_1 L_u^{-b_2} d_\ell\right)^2}\right) \tag{7}$$

where the best fit parameters relating a and b to σ/U and L_u are a_1 = 8.4, a_2 = 0.05, b_1 = 0.25, and b_2 = 1.24. Examples of coherence curves using the model in (7) are provided by the red curves in Fig. 3.

Several interesting trends are revealed by the developed longitudinal coherence function. First, if the impact of L_u is ignored, relative changes in U will affect coherence more than relative changes in d_ℓ due to the dependence of the a parameter on mean wind speed. This behavior is also present in the Kristensen model, but not in the Pielke and Panofsky formula, which depends on d_ℓ and U only through d_ℓ/U. Second, as integral length scale decreases and more of the energy in the wind is concentrated at small length scales, the value of coherence approached as f approaches 0 decreases as well. Since stable boundary layers tend to produce small length scales, as revealed by Fig. 4, low frequency coherence decreases during stable conditions. Finally, as can be seen in Fig. 3, the coherence model is unable to capture the sharp decrease in coherence above a certain frequency apparent in the stable condition as well as for the 31.5 m separation in the neutral condition. The developed model could be improved

by including an additional term to allow for faster decay at high frequencies. To summarize the quality of fit for the developed coherence model, Table II contains errors based on the objective function in (5) for each wind condition.

TABLE II

ERRORS BETWEEN THE DEVELOPED COHERENCE MODEL IN (7) AND THE LES-BASED COHERENCE CURVES, CALCULATED USING (5).

ID	1	2	3	4	5	6
Model Error ($\times 10^{-3}$)	3.4	4.2	11.4	17.8	7.3	6.9
ID	7	8	9	10	11	12
Model Error ($\times 10^{-3}$)	2.4	12.4	3.6	7.7	7.5	10.7

IV. LIDAR MEASUREMENT SCENARIO OPTIMIZATION

In this section, the longitudinal coherence model presented in (7) is combined with a statistical frequency-domain wind field model describing transverse and vertical spatial coherence along with the turbulence power spectra. The complete wind field model is then used to optimize a lidar measurement scenario to minimize measurement error for a range of mean wind speeds and turbulence intensities.

A. Lidar Measurement Scenario

As shown in Fig. 5, the measurement scenario analyzed here consists of three circularly-scanning lidar beams using lidars located at the turbine hub [5]. The lidar beams are focused at a preview distance d upstream of the rotor on a scan circle with radius r, and rotate at the same speed as the turbine rotor. Each lidar beam measures the wind that will encounter a particular blade after propagating downstream from the measurement plane. A model of the continuous-wave (CW) ZephIR lidar [6] is used to determine the inherent spatial averaging, or range weighting, along the lidar beam illustrated by the magenta curves in Fig. 5. An estimate of the rotor effective wind speed u_{eff} is formed by averaging the three lidar measurements at every time step, using the ZephIR's sampling rate of 50 Hz. Rotor effective wind speed u_{eff} [7] is defined as the time-varying average of the three rotating blade effective wind speeds u_{blade}. Blade effective wind speed is calculated as the average u component of wind speed, which has the greatest impact on rotor aerodynamics, along the length of the blade weighted by the spanwise contribution to aerodynamic torque production:

$$u_{blade} = \frac{\int_0^R u\left(s\right) C_Q\left(s\right) sds}{\int_0^R C_Q\left(s\right) sds} \tag{8}$$

where s represents the radial distance from the rotor hub, R is the rotor radius, and $C_Q\left(s\right)$ is the coefficient of torque as a function of spanwise position calculated using the blade element momentum method included in NREL's AeroDyn code [23] with the NREL 5-MW reference turbine parameters [17]. In order to estimate the u component of wind speed, by assuming the v and w components are zero, the line-of-sight lidar measurements are divided by $\cos\theta = d/\sqrt{d^2+r^2}$, where θ is the angle between the lidar beam and the mean wind direction [6].

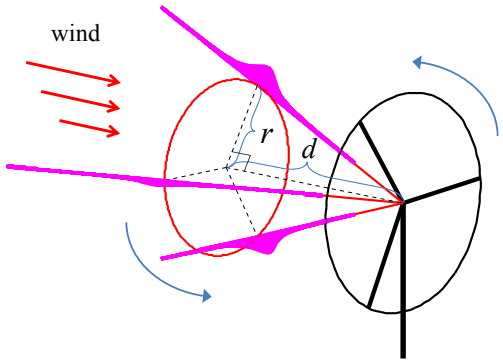

Fig. 5. Hub-mounted lidar measurement scenario. Three lidar beams scan a measurement circle at a distance d upstream of the turbine with a radius r. The lidar beams rotate at the same speed as the turbine rotor.

For a variety of mean wind speeds and turbulence intensities, the optimal scan radius r and preview distance d are found that minimize the mean square error (MSE) between the lidar-based estimate of the rotor effective wind speed $\hat{u}_{eff}$ and the true wind speed u_{eff} at the turbine. Assuming that $\hat{u}_{eff}$ is optimally filtered using a minimum-MSE Wiener prefilter based on the correlation between the measured and true wind speeds [7], the MSE can be written as a function of the measurement coherence and the PSD of u_{eff}:

$$\text{MSE} = \int_0^{f_{max}} S_{u_{eff},u_{eff}}\left(f\right)\left(1-\gamma^2_{u_{eff},\hat{u}_{eff}}\left(f\right)\right) df, \tag{9}$$

where an integration limit of f_{max} = 1 Hz is used [8], [10].

The expression (9) is calculated in the frequency domain for each combination of atmospheric and lidar variables using a statistical frequency-domain model of the wind field. The power spectra of the u, v, and w components are defined as Kaimal turbulence spectra [16] containing the ratios σ_v/σ_u and σ_w/σ_u as well as the integral length scale values calculated from the LES wind fields. Spatial coherence in the transverse and vertical plane, perpendicular to the wind direction, is calculated using an expression based on (4) specified in the IEC standard [16], [22]. Longitudinal spatial coherence is described using (7). Spatial coherence between wind speeds with separations both in the longitudinal and transverse-vertical directions is similarly treated as an exponential decay formula with the decay constant defined as the square root of the sum of the squared longitudinal and transverse-vertical coherence decay constants. Using the range weighting function for the ZephIR CW lidar [6], and C_Q values calculated using blade element momentum theory, the measurement coherences $\gamma^2_{u_{eff},\hat{u}_{eff}}\left(f\right)$ and PSDs $S_{u_{eff},u_{eff}}\left(f\right)$ used to determine the MSE are calculated using frequency-domain techniques explained in [8] and [9].

B. Measurement Scenario Optimization

The co-dependent optimal scan radii and preview distances, as well as the corresponding achievable MSE normalized by the integral of the PSD of u_{eff} (equivalent to the

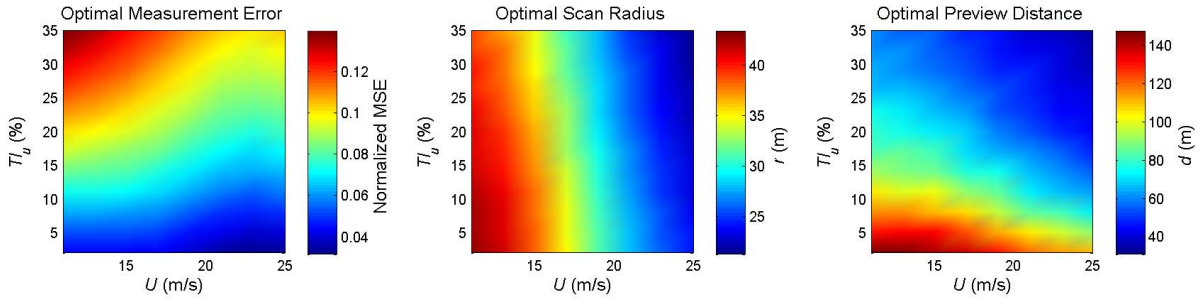

Fig. 6. Minimum achievable MSE calculated with (9) normalized by the variance of u_{eff} along with the combined optimal scan radii and preview distances as a function of mean wind speed and turbulence intensity using σ_v/σ_u = 0.72, σ_w/σ_u = 0.59, and L_u = 230 m from unstable wind field 11.

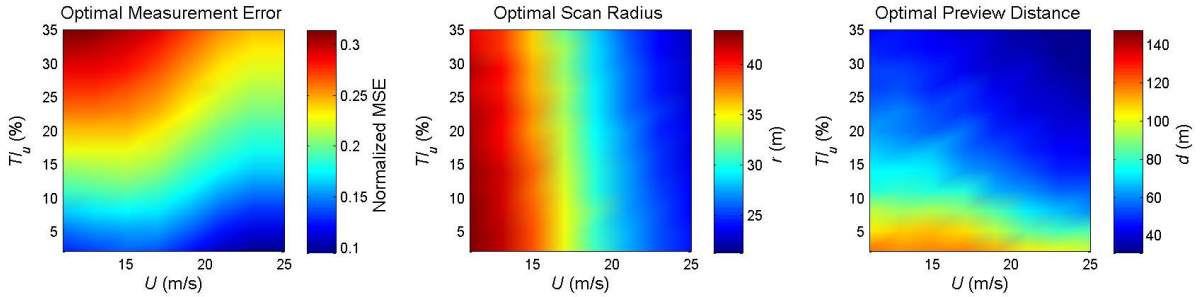

Fig. 7. Minimum achievable MSE calculated with (9) normalized by the variance of u_{eff} along with the combined optimal scan radii and preview distances as a function of mean wind speed and turbulence intensity using σ_v/σ_u = 0.73, σ_w/σ_u = 0.55, and L_u = 56 m from stable wind field 12.

variance of u_{eff}), are found as a function of U and TI_u using the σ_v/σ_u and σ_w/σ_u ratios and integral length scales for LES wind fields 11 and 12. These unstable and stable wind fields allow the dependence of the optimal lidar measurement scenario on turbulence length scale to be explored. Fig. 6 contains the MSEs and optimal r and d values representative of the unstable length scale in wind field 11 while Fig. 7 displays the optimization results for wind field 12.

Both figures illustrate the same general trends. As U increases above 11.4 m/s, rated wind speed for the 5-MW reference turbine, the blades are pitched to maintain constant power capture [17]. This shifts aerodynamic torque production away from the outboard section of the blades toward the root. Thus the optimal scan radius tends to decrease, tracking the spanwise region of the blades with the greatest impact on power production. Errors caused by the v and w wind components contributing to the measured line-of-sight velocity, which we call the directional bias error, decrease as r/d decreases and the beam direction becomes more aligned with the longitudinal direction. Therefore, as the optimal r becomes smaller, the optimal d decreases as well allowing lower measurement error due to less wind evolution without significantly increasing r/d. This reduction in measurement error due to shorter preview distances is augmented by the wind evolution becoming less severe as U increases. As turbulence intensity increases, the optimal preview distance drops to counter the intensifying wind evolution. The drop in d produces very minor decreases in the optimal r to help reduce the resulting higher directional bias errors. However, the net increase in directional bias error combined with the intensification of wind evolution causes the minimum achievable MSE to increase as turbulence intensity grows. A comparison of Figs. 6 and 7 reveals that measurement quality suffers as the length scale of turbulence decreases, due to the drop in low-frequency coherence. Accordingly, due to the increased wind evolution, the optimal d are shorter.

The results presented in Figs. 6 and 7 have two important implications for the design of feedforward wind turbine control systems. First of all, measurement accuracy can be improved by using a lidar system with variable preview distance; the optimal d values revealed in this study range from 31 m to 147 m. For example, preview distance could be varied based on knowledge of the mean wind speed and estimates of the turbulence intensity and length scale. The optimal scan radius, on the other hand, depends primarily on the mean wind speed via its impact on torque production along the blades, and would be easy to schedule as a function of blade pitch angle alone. Second, the optimal MSE values presented are achieved using an optimal measurement prefilter (H_{pre} in Fig. 1), which is a function of the measurement coherence $\gamma^2_{u_{eff},\hat{u}_{eff}}(f)$. Because $\gamma^2_{u_{eff},\hat{u}_{eff}}(f)$ depends on the amount of wind evolution, feedforward controller designs can benefit from adaptive prefiltering. While the filter coefficients could be varied based on estimated atmospheric variables, they could also be formed by directly calculating the coherence between the lidar measurements and the estimated wind disturbance encountered by the turbine [10].

V. Discussion and Conclusions

This paper presented a wind evolution model based on spatial coherence curves measured in a variety of LES wind fields. A longitudinal spatial coherence formula, based on

the equation suggested by Thresher *et al.* [15] for transverse and vertical coherence was developed that depends on mean wind speed, turbulent kinetic energy, and integral length scale. This longitudinal coherence formula was combined with a frequency-domain wind field model described in the IEC standard [16], [22] to determine the mean square measurement error for a hub-mounted, circularly-scanning CW lidar system used with the NREL 5-MW reference turbine. Calculations of MSE for various mean wind speeds and turbulence intensities with integral length scales representative of unstable and stable conditions revealed that the optimal lidar preview distance, circular scan radius, and measurement quality depend strongly on the specific atmospheric conditions. The results suggest that preview-based wind turbine control systems can benefit from lidar systems with variable scan geometries and adaptive prefilters. It should be noted that for certain wind conditions the optimal preview distance is as short as 30.7 m (providing less than 1.25 seconds of preview time for U = 25 m/s). In practice, a preview time of several seconds is required by the controller to allow for filtering the lidar measurements and to account for blade pitch actuator delay [2].

As illustrated in Fig. 3 as well as Table II, the developed wind evolution model matches the measured coherence curves very well for certain wind conditions (e.g., unstable wind field 5), and not as well for others (e.g., stable wind field 3). Additional improvements can be made to the coherence formula, such as introducing a term to account for the sharp decline in coherence at high frequencies visible for wind field 3. Furthermore, validation of the evolution model would benefit from wind conditions with higher mean wind speeds and larger ratios of σ/U. The results presented in Section IV were generated for mean wind speeds up to 25 m/s and σ/U ratios up to 0.48, while the LES wind fields only contained values of U up to $\sim$12 m/s and σ/U ratios up to 0.23. Moreover, while the developed wind evolution model is applicable to preview-based individual turbine control scenarios, it is uncertain whether it can be extended to wind plant-scales of the order of tens of rotor diameters. Coherence calculations with greater frequency resolution, capable of revealing the correlation at very low frequencies, using wind fields with much larger longitudinal separations could be used to either validate the presented model for wind plant-scale applications or develop a more appropriate model.

Finally, while combining a longitudinal coherence formula with an existing transverse-vertical coherence model is convenient for forming a simplified statistical definition of a wind field, other methods of defining spatial coherence in all three dimensions exist. For example, a spectral wind field definition developed by Wilczek *et al.* [24] describes coherence in all three spatial dimensions using one unifying formula, although the relevant spatial scales in [24] are too large to be applied to individual-turbine control scenarios.

REFERENCES

[1] J. Laks, L. Pao, A. Wright, N. Kelley, and B. Jonkman, "The use of preview wind measurements for blade pitch control," *Mechatronics*, vol. 21, no. 4, pp. 668–681, Jun. 2011.

[2] F. Dunne, D. Schlipf, L. Y. Pao, A. D. Wright, B. Jonkman, N. Kelley, and E. Simley, "Comparison of two independent lidar-based pitch control designs," in *Proc. 50th AIAA Aerospace Sciences Meeting*, Nashville, TN, Jan. 2012.

[3] E. A. Bossanyi, "Un-freezing the wind: improved wind field modelling for investigating lidar-assisted wind turbine control," in *Proc. European Wind Energy Association*, Copenhagen, Denmark, Apr. 2012.

[4] J. Laks, E. Simley, and L. Pao, "A spectral model for evaluating the effect of wind evolution on wind turbine preview control," in *Proc. American Control Conference*, Washington, D.C., Jun. 2013.

[5] T. Mikkelsen, N. Angelou, K. Hansen, M. Sjöholm, M. Harris, C. Slinger, P. Hadley, R. Scullion, G. Ellis, and G. Vives, "A spinner-integrated wind lidar for enhanced wind turbine control," *Wind Energy*, vol. 16, no. 4, pp. 625–643, 2013.

[6] E. Simley, L. Y. Pao, R. Frehlich, B. Jonkman, and N. Kelley, "Analysis of light detection and ranging wind speed measurements for wind turbine control," *Wind Energy*, vol. 17, no. 3, 2014.

[7] E. Simley and L. Y. Pao, "Reducing LIDAR wind speed measurement error with optimal filtering," in *Proc. American Control Conference*, Washington, D.C., Jun. 2013.

[8] ——, "Correlation between rotating LIDAR measurements and blade effective wind speed," in *Proc. 51st AIAA Aerospace Sciences Meeting*, Grapevine, TX, Jan. 2013.

[9] D. Schlipf, J. Mann, and P. Cheng, "Model of the correlation between lidar systems and wind turbines for lidar-assisted control," *J. Atmos. and Ocean. Tech.*, vol. 30, no. 10, pp. 2233–2240, 2013.

[10] E. Simley, L. Pao, P. Gebraad, and M. Churchfield, "Investigation of the impact of the upstream induction zone on LIDAR measurement accuracy for wind turbine control applications using large-eddy simulation," in *Proc. Science of Making Torque from Wind*, Lyngby, Denmark, Jun. 2014.

[11] A. G. Davenport, "The spectrum of horizontal gustiness near the ground in high winds," *J. Roy. Meteor. Soc.*, vol. 87, pp. 194–211, 1961.

[12] R. A. Pielke and H. A. Panofsky, "Turbulence characteristics along several towers," *Boundary-Layer Meteorology*, vol. 1, no. 2, pp. 115–130, 1970.

[13] L. Kristensen, "On longitudinal spectral coherence," *Boundary-Layer Meteorology*, vol. 16, no. 2, pp. 145–153, 1979.

[14] M. Churchfield and S. Lee. (2014, Sep.) NWTC Information Portal (SOWFA). National Renewable Energy Laboratory. [Online]. Available: https://wind.nrel.gov/SOWFA/

[15] R. Thresher, W. Holley, C. Smith, N. Jafarey, and S.-R. Lin, "Modeling the response of wind turbines to atmospheric turbulence," Department of Mechanical Engineering, Oregon State University, RL0/2227-81/2, Corvallis, OR, Tech. Rep., Aug. 1981.

[16] B. Jonkman, "TurbSim user's guide: Version 1.50," National Renewable Energy Laboratory, NREL/TP-500-46198, Golden, CO, Tech. Rep., 2009.

[17] J. Jonkman, S. Butterfield, W. Musial, and G. Scott, "Definition of a 5-MW reference wind turbine for offshore system development," National Renewable Energy Laboratory, NREL/TP-500-38060, Golden, CO, Tech. Rep., 2009.

[18] "OpenFOAM the open source CFD toolbox, user's manual, version 1.7.1," OpenCFD, Reading, UK, Tech. Rep., 2010.

[19] M. J. Churchfield, S. Lee, J. Michalakes, and P. J. Moriarty, "A numerical study of the effects of atmospheric and wake turbulence on wind turbine dynamics," *J. Turb.*, vol. 13, no. 14, pp. 1–32, 2012.

[20] M. J. Churchfield, S. Lee, and P. J. Moriarty, "Adding complex terrain and stable atmospheric condition capability to the OpenFOAM-based flow solver of the simulator for on/offshore wind farm applications (SOWFA)," in *Proc. 1st Symposium on OpenFOAM in Wind Energy*, Oldenburg, Germany, Mar. 2013.

[21] S. Kay, *Modern Spectral Estimation: Theory and Application*. Englewood Cliffs, NJ: Prentice Hall, 1999.

[22] "IEC 61400-1 'Wind turbines-part 1: Design requirements.' 3rd edition," International Electrotechnical Commission, Geneva, Switzerland, Tech. Rep., 2005.

[23] P. Moriarty and A. Hansen, "AeroDyn theory manual," National Renewable Energy Laboratory, NREL/TP-500-36881, Golden, CO, Tech. Rep., Jan. 2005.

[24] M. Wilczek, R. Stevens, Y. Narita, and C. Meneveau, "A wavenumber-frequency spectral model for atmospheric boundary layers," in *Proc. Science of Making Torque from Wind*, Lyngby, Denmark, Jun. 2014.